Charged Bose condensate screening of hydrogenic impurities in two and three dimensions

1999 J. Phys.: Condens. Matter 11 2363

(http://iopscience.iop.org/0953-8984/11/11/008)

J. Phys.: Condens. Matter **11** (1999) 2363–2378. Printed in the UK PII: S0953-8984(99)99470-5

Charged Bose condensate screening of hydrogenic impurities in two and three dimensions

A Gold† and A Ghazali‡

† Centre d'Elaboration de Matériaux et d'Etudes Structurales (CEMES-CNRS), 29 Rue Jeanne Marvig, 31055 Toulouse, France
‡ Groupe de Physique des Solides, UMR 7588-CNRS, Universités Paris 7 et 6, 2 place Jussieu, 75251 Paris, France

Received 19 November 1998

Abstract. We study screening effects of a three- and two-dimensional charged Bose condensate on the binding energy of a hydrogenic impurity. Many-body effects are taken into account via a local-field correction. The variational method and the matrix diagonalization method are used to calculate the energies of the ground state and of excited states as functions of the condensate density. With increasing boson density the binding energies decrease and vanish at a critical density. For a given density, Bose condensate screening is found to be more efficient than electron screening and the binding energies vanish at a lower density than for electron screening.

1. Introduction

The reduction of the binding energy of a hydrogenic impurity due to electron screening was studied extensively in the past [1–9]. Such calculations are important for impure metals and doped semiconductors. The binding energy was calculated by using different approximations for the screening function. The effect of screening by an electron gas on a single charged impurity in three dimensions (3D) [1–6] and in two dimensions (2D) [5–9] was considered. In 3D it was found that the binding energy of a positively charged impurity vanishes if the screening density of electrons is larger than a critical density, the Mott density. In contrast to this it was shown in 2D that the binding energy is always finite, even if the electron density becomes very high [8].

In this paper we consider the binding energy of a single hydrogenic impurity screened by a charged Bose condensate (BC) in 3D and 2D. A 2D charged BC might be considered as a model for high-T_c superconductors [10]. A 3D charged BC has applications in astrophysics [11]. The recent discovery of Bose condensation of atoms (neutral particles) and the observation of collective modes [12] has motivated a huge theoretical activity in order to understand better the physical properties of BCs.

A charged BC is a basic system in statistical physics where many-body effects are currently studied [13–21]. Of special interest are the screening properties of a BC and how they compare with the screening properties of an electron gas. The screening effects of a BC on the binding energy of a hydrogenic impurity represent a new version of screening for a known physical problem. Comparing with screening properties of an electron gas, we find for boson screening new quantitative and qualitative results in 3D and in 2D.

0953-8984/99/112363+16$19.50

In the present paper we show how the random-phase approximation (RPA) [22], which is the mean-field approximation, is modified by correlation effects. These many-body effects are described by the local-field correction (LFC). The LFC is important to get correct expressions for the test-charge–boson and test-charge–test-charge interactions when the screening gas density is not high enough for the RPA to be valid [22].

In section 2 we describe the model and the theory. The results of a single hydrogenic impurity screened by a 3D-BC are described in section 3. The corresponding results for a 2D-BC are given in section 4. Our results are discussed in section 5 and we conclude in section 6.

2. Model and theory

2.1. Model

As the model system we use a Bose gas with a parabolic dispersion and density N_d in dimension $d = 3$ and $d = 2$. All particles are assumed to have condensed to the lowest energy and form a BC. Distances are expressed in units of the effective Bohr radius $a^* = \varepsilon_L/m^*e^2$ with the Planck constant $h/2\pi = 1$. m^* is the effective mass of the bosons and ε_L is the dielectric constant of the background material. Energy values are expressed in units of the effective Rydberg $\mathrm{Ry}^* = m^*e^4/2\varepsilon_L^2$. The density parameter r_s is given by $r_s = [3/4\pi N_3 a^{*3}]^{1/3}$ for 3D and by $r_s = [1/\pi N_2 a^{*2}]^{1/2}$ for 2D.

We consider a jellium model: we assume that the BC is negatively charged and a homogeneous positive background charge ensures charge neutrality. The Coulomb interaction potential between the bosons is given in the Fourier space by $V(q) = 4\pi e_2/\varepsilon_L q^2$ in 3D and by $V(q) = 2\pi e^2/\varepsilon_L q$ in 2D. The Coulomb interaction potential between two particles with opposite charges is attractive and given by the bare (b) Coulomb potential $V_b(q) = -V(q)$.

In the following we study the test-charge–test-charge and the test-charge–boson interactions. For simplicity, the Bose particles and test-charges are assumed to hold an elementary charge $\pm e$. For specific cases, the effective Bohr radius and the effective Rydberg, defined above, should be rescaled according to the charges and masses under consideration.

2.2. The screened Coulomb interaction

The screened test-charge–test-charge (tt) interaction $V_{tt,sc}(q)$ is given in terms of the screening function $\varepsilon_{tt}(q)$ by

$$V_{tt,sc}(q) = \frac{V_b(q)}{\varepsilon_{tt}(q)}. \tag{1}$$

We assume that the two *test-charges* are distinct from the boson gas providing the screening. The dielectric function $\varepsilon_{tt}(q)$ is given by $1/\varepsilon_{tt}(q) = [1 - V(q)G(q)X_0(q)]/[1 + V(q)[1 - G(q)]X_0(q)]$ where $G(q)$ is the LFC.

$X_0(q) = 4Nm^*/q^2$ is the static density–density response function of the free BC [13]. The divergent behaviour of the response function of the BC for $q \to 0$ is due to the Bose condensation of the particles. For small wavenumbers the static density–density response function of a free BC is much larger than for a free electron gas, where $X_0(q \to 0) = \rho_F$ and ρ_F is the density of states at the Fermi energy.

The screened test-charge–boson (tb) interaction $V_{tb,sc}(q)$ is written as

$$V_{tb,sc}(q) = \frac{V_b(q)}{\varepsilon_{tb}(q)}. \tag{2}$$

For the test-charge–boson (tb) interaction one gets $1/\varepsilon_{tb}(q) = 1/[1 + V(q)[1 - G(q)]X_0(q)]$. In fact, the expressions for $1/\varepsilon_{tt}(q)$ and $1/\varepsilon_{tb}(q)$ were derived [23] for electron screening, but it can be shown easily that they also hold for screening due to Bose particles.

In the following we use $G_2(q)$ and $G_3(q)$ for the LFC in 2D and 3D, respectively. For 3D the dielectric function for the test-charge–test-charge interaction is given by

$$\frac{1}{\varepsilon_{tt}(q)} = \frac{1 - G_3(q)q_3^4/q^4}{1 + q_3^4[1 - G_3(q)]/q^4} \tag{3a}$$

with $q_3 a^* = 12^{1/4}/r_s^{3/4}$. $1/q_3$ is the relevant length scale for screening in the 3D-BC and depends on the density via r_s. The dielectric function in 2D is expressed as

$$\frac{1}{\varepsilon_{tt}(q)} = \frac{1 - G_2(q)q_2^3/q^3}{1 + q_2^3[1 - G_2(q)]/q^3} \tag{3b}$$

with $q_2 a^* = 2/r_s^{2/3}$ and $1/q_2$ is the relevant length scale for screening in the 2D-BC.

For the test-charge–boson interaction one finds

$$\frac{1}{\varepsilon_{tb}(q)} = \frac{1}{1 + q_3^4[1 - G_3(q)]/q^4} \tag{4a}$$

in 3D and

$$\frac{1}{\varepsilon_{tb}(q)} = \frac{1}{1 + q_2^3[1 - G_2(q)]/q^3} \tag{4b}$$

in 2D.

For $r_s \ll 1$ the LFC can be neglected. With $G(q) = 0$ one then gets the familiar RPA expression $\varepsilon_{RPA}(q) = 1 + V(q)X_0(q)$ with $V_{RPA}(q) = V_b(q)/\varepsilon_{RPA}(q)$ and the three dielectric functions are equal: $\varepsilon_{tt}(q) = \varepsilon_{tb}(q) = \varepsilon_{RPA}(q)$. For $r_s > 1$ $\varepsilon_{tb}(q)$ takes a different form than $\varepsilon_{tt}(q)$ to account for the indistinguishability of the bosons.

In our calculation of the LFC we use the sum-rule approximation [19] of the Singwi–Tosi–Land–Sjölander (STLS) approach [24]. In the sum-rule approach the LFC is parametrized by three coefficients $C_{id}(r_s)$ ($i = 1, 2, 3$). For the 3D-BC the LFC is written as

$$G_3(q) = r_s^{3/4} \frac{0.846q^2}{2.188q_3^2 C_{13}(r_s) + q^2 C_{23}(r_s) - q_3 q C_{33}(r_s)}. \tag{5a}$$

For the 2D electron gas the LFC is given by

$$G_2(q) = r_s^{2/3} \frac{1.402q}{[2.644q_2^2 C_{12}(r_s)^2 + q^2 C_{22}(r_s)^2 - q_2 q C_{32}(r_s)]^{1/2}}. \tag{5b}$$

The coefficients are determined as for electrons [25]. $C_{1d}(r_s)$ is determined from the compressibility of the condensate calculated within the STLS approach. The STLS approach describes the pair correlation function $g(r = 0)$ by the LFC for large wave numbers via $G(q \to \infty) = 1 - g(r = 0)$: this defines $C_{2d}(r_s)$. The coefficient $C_{3d}(r_s)$ is calculated using the relation between $g(r = 0)$ and the static structure factor. Therefore the LFC fulfils the compressibility sum rule. Details will be published elsewhere [26].

2.3. Bound states

The Schrödinger equation for a particle with reduced mass m^* in the screened potential is solved numerically in the momentum space. The Schrödinger equation in the momentum space is given by

$$\frac{q^2}{2m^*}\psi(\boldsymbol{q}) + \frac{1}{(2\pi)^d}\int \mathrm{d}^d\boldsymbol{q}' V_{sc}(\boldsymbol{q} - \boldsymbol{q}')\psi(\boldsymbol{q}') = E\psi(\boldsymbol{q}). \tag{6}$$

The equation (6) is suitably discretized according to $\boldsymbol{q}$ and $\boldsymbol{q}'$ under the form of a matrix. In equation (6) and in the following $V_{sc}(q)$ represents $V_{RPA}(q)$, $V_{tb,sc}(q)$ or $V_{tt,sc}(q)$. The eigenenergy and eigenfunction problem is then solved numerically by a standard method for matrix diagonalization. Details can be found in [5].

For 3D the wave function $\psi(\boldsymbol{r})$ is given by $\phi_{n_r l}(r)Y_{lm}(\varphi,\theta)$. The degeneracy of these states is $g_l = 2l+1$. $\phi_{n_r l}(r)$ is the solution of the radial Schrödinger equation for the effective potential $V_{eff}(r) = V_l(r) + V_{sc}(r)$ with $V_l(r) = l(l+1)/2m^*r^2$. For 2D, $\psi(\boldsymbol{r}) = \phi_{n_r l}(r)\exp[\pm \mathrm{i}l\varphi]$ with degeneracy $g_l = 1$ for $l = 0$ and $g_l = 2$ for $l > 0$. $\phi_{n_r l}(r)$ is the radial function for the effective potential $V_{eff}(r) = V_l(r) + V_{sc}(r)$ with $V_l(r) = l^2/2m^*r^2$. In the momentum space the wave function is written in the same way as in the real space as $\psi(\boldsymbol{q}) = \phi_{n_r l}(q)\exp(\pm \mathrm{i}l\varphi)$. In the following we will use $\phi(r)$ instead of $\phi_{n_r l}(r)$.

For the bound state energies, we find excellent agreement between the matrix diagonalization method and the variational method. For the ground state, the 1s state, we use

$$\phi_{1v}(r) = A\,\mathrm{e}^{-r/2\nu} \tag{7}$$

with the variational parameter ν. For the first excited state, the 2s state, we use

$$\phi_{2v}(r) = A(1 - rD)\,\mathrm{e}^{-r/2\kappa} \tag{8a}$$

with κ as the variational parameter. D is determined by the condition $\langle\phi_{1v}|\phi_{2v}\rangle = 0$. For the second excited state, the 2p state, we use

$$\phi_{3v}(r) = Ar\mathrm{e}^{-r/2\mu} \tag{8b}$$

with μ as the variational parameter. All these variational wave functions are *hydrogenic-like* wave functions where the spatial extension parameters ν, κ and μ are variational.

In the following we present results for bound states using the RPA, the tb- and the tt-interaction. In general we only find bound states for r_s larger than a critical value r_{sc}. The RPA results demonstrate the importance of many-body effects described by the LFC.

3. Results for three dimensions

3.1. The screened potential

In the real space the screened Coulomb interaction in 3D is given by

$$V_{sc}(r) = \frac{1}{2\pi^2 r}\int_0^\infty \mathrm{d}q\, q\,\sin(qr)V_{sc}(q). \tag{9}$$

Within the RPA the screened potential can be calculated analytically. Putting $x = rq_3$ one obtains

$$V_{RPA}(x) = -\frac{2\mathrm{Ry}^* 12^{1/4}}{r_s^{3/4}}\left\{\frac{1}{x}\exp(-x/2^{1/2})\cos(x/2^{1/2})\right\}. \tag{10}$$

The energy scale of $V_{RPA}(x)$ depends on $\mathrm{Ry}^*/r_s^{3/4}$, while the characteristic length r_0 is given by $x_0 = r_0 q_3 \approx 1$, which means $r_0 \approx 1/q_3 \propto r_s^{3/4}$. $V_{RPA}(r)$ shows very interesting features, namely (i) Coulomb attraction at small distances, (ii) exponential screening at intermediate distances and (iii) oscillating behaviour at large distances. It merits on its own a detailed study. For the BC the characteristic length r_0 is related to the density of the condensate through r_s. We mention that for electron screening within the RPA the screened potential exhibits the same features. In particular, Friedel's oscillations also define a characteristic length given by $r_0 k_F \approx 1$, i.e. $r_0 \approx 1/k_F \propto r_s$. Here k_F is the wavenumber at the Fermi level. However, in

the electron case, V_{RPA} cannot be given in analytical form. Therefore, the charged BC is a useful model system to discuss screening effects in quantum liquids.

The screened potential can be characterized by four lengths r_i ($i = 1$–4), which are all connected to r_0: $V_{RPA}(r)$ has a Coulomb singularity for $r \to 0$, $V_{RPA}(r_1) = 0$ for

$$r_1/a^* = 1.194 r_s^{3/4} \tag{11a}$$

it shows a maximum $V_{RPA}(r_2)/\mathrm{Ry}^* = 0.0781/r_s^{3/4}$ for $r_2/a^* = 1.650 r_s^{3/4}$, it vanishes again $V_{RPA}(r_3) = 0$ for $r_3/a^* = 3.581 r_s^{3/4}$, and it shows a minimum

$$V_{RPA}(r_4)/\mathrm{Ry}^* = -0.001\,39/r_s^{3/4} \tag{11b}$$

for

$$r_4/a^* = 4.113 r_s^{3/4}. \tag{11c}$$

At very low densities, corresponding to $r_s \to \infty$ or $q_3 \to 0$, the potential is unscreened and the bound state energies are those of the 3D hydrogen atom: the 1s state has a binding energy of $-1\mathrm{Ry}^*$ and a spatial extension $\nu = 0.5a^*$. The length r_1 is a good criterion for screening: if $r_1 < a^*$ a strong reduction of the binding energy is expected due to screening effects.

$V_{sc}(r)$ versus r is shown in figure 1 for $r_s = 2$. For $r_s = 2$ the differences between $V_{RPA}(r)$, $V_{tb,sc}(r)$ and $V_{tt,sc}(r)$ are small, however already visible. For very small distances the Coulomb attraction becomes dominant. The values r_1 and r_2 can be seen in figure 1 and exist for $V_{RPA}(r)$, $V_{tb,sc}(r)$ and $V_{tt,sc}(r)$.

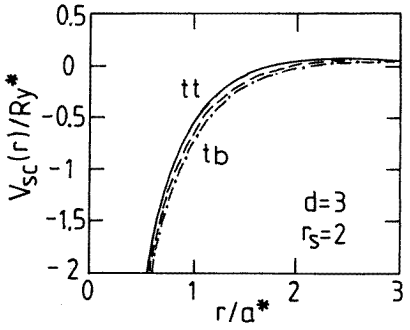

Figure 1. Screened potential $V_{sc}(r)$ versus distance r for $r_s = 2$ in 3D. The solid and dot–dashed line represents the test-charge–test-charge (tt) and the test-charge–boson (tb) interaction, respectively. The dashed line represents the RPA.

3.2. Bound states within the RPA

Within the variational approach, the binding energies of the 1s state, and for the 2s and 2p states for some large r_s values, are given in table 1 for boson screening and electron screening. It is interesting to note that the binding energies for low densities are independent of the statistical properties of the quantum liquid that supplies the screening.

For $r_s < 4$ the BC screening is more efficient than the electron screening and the binding energy vanishes at a higher r_s-value; see table 1. The r_s-value for which the binding energy vanishes is denoted as the critical density parameter r_{sc}, see figure 2. Obviously, r_{sc} depends on the bound state which we consider. The smallest value for r_{sc} is found for the ground state. The corresponding density is called Mott's [1] critical density N_{3c}, originally found for electrons. It is given by $N_{3c}^{1/3}a^* = (3/4\pi)^{1/3}/r_{sc}$. For the 1s-state in a BC we get $N_{3c}^{1/3}a^* = 0.24$. For the excited states the values for r_{sc} are also given in table 1.

Table 1. Binding energies in 3D for the 1s, 2s and 2p state found by the variational method within the RPA for screening by charged bosons and by charged fermions [5]. In the last row we give the values r_{sc} where the binding energy vanishes.

	Boson binding energy (Ry*)			Fermion binding energy (Ry*)		
r_s	1s	2s	2p	1s	2s	2p
3	−0.061	—	—	−0.095	—	—
5	−0.292	—	—	−0.289	—	—
10	−0.551	—	—	−0.537	—	—
20	−0.726	−0.019	−0.008	−0.716	−0.012	−0.001
40	−0.836	−0.096	−0.093	−0.830	−0.091	−0.088
100	−0.917	−0.168	−0.168	−0.915	−0.167	−0.166
1000	−0.985	−0.235	−0.235	−0.985	−0.235	−0.235
r_{sc}	2.595	16.9	18.8	2.12	17.8	19.8

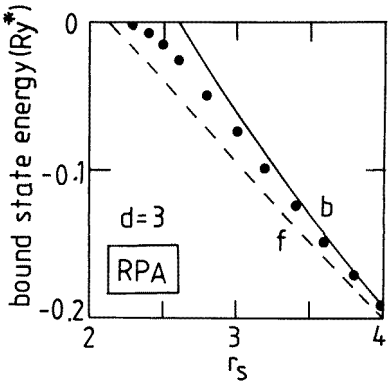

Figure 2. Binding energy for the 1s state versus r_s within the RPA for boson (solid line) and fermion (dashed line) screening in 3D from the variational calculation. Our results from the matrix diagonalization are shown as solid points.

3.3. Bound states including many-body effects: tb

Many-body effects described by the LFC play an important role for the binding energy. This is demonstrated in figure 3 for the 1s state. At a given value of r_s, we find the largest binding energy for the tb-interaction. The binding energy is smallest for the tt-interaction.

For the tb-interaction (and the RPA) the results for the binding energy of the 2s and the 2p state versus r_s are shown in figure 4. The binding energy of the excited states vanishes for r_s near 12. Note that the 2s and 2p states are not degenerate. The screening effect breaks the accidental degeneracy found in the hydrogen atom. In the unscreened limit for $r_s \to \infty$, the binding energy of the first excited states become $-\mathrm{Ry}^*/4$ with $\kappa = \mu = a^*$ as for the hydrogen atom; see equations (8*a–b*). Higher excited states, 3s, 3p,... have not been found for $r_s < 50$. The variational parameters ν, κ and μ increase with decreasing r_s. For instance, within the RPA for the 1s state ν increases from $a^*/2$ for $r_s \to \infty$ to $0.69a^*$ for $r_s = r_{sc} = 2.6$.

3.4. Bound states with the local field correction: tt

The results for the 1s state for the tt-interaction are shown in figure 3. The binding energies are smaller than within the RPA. The 1s state is described by a hydrogenic-like wave function;

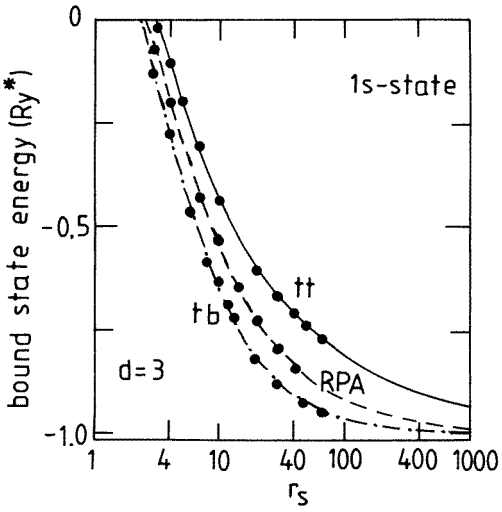

Figure 3. Binding energy for the 1s state versus r_s within the RPA (dashed line), the tb-interaction (dashed–dotted line) and the tt-interaction (solid line) in 3D from the variational calculation. Our results from the matrix diagonalization are shown as solid points.

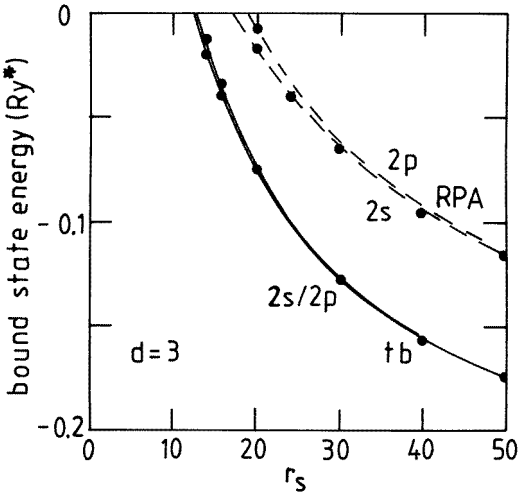

Figure 4. Binding energy for the 2s and the 2p state versus r_s for the tb-interaction and the RPA in 3D from the variational calculation. Our results from the matrix diagonalization are shown as solid points.

note the good agreement between the matrix diagonalization method and the variational method.

With the variational wave function $\phi_{2v}(r)$ and $\phi_{3v}(r)$ for the hydrogenic-like 2s and the 2p states we found no excited states for $r_s < 50$. However, with the matrix method we found excited states for $r_s > 22$. Therefore we studied $V_{tt,sc}(r)$ in detail. In fact, we found that due to many-body effects the attraction $V_{tt,sc}(r)$ at r_4 is strongly increased for $r_s > 1$ compared to the RPA result, see figure 5. There we have shown $V_{tt,sc}(r_4)$ versus r_s. Note that binding energies larger than 10mRy* cannot be explained by $V_{tt,sc}(r_4)$.

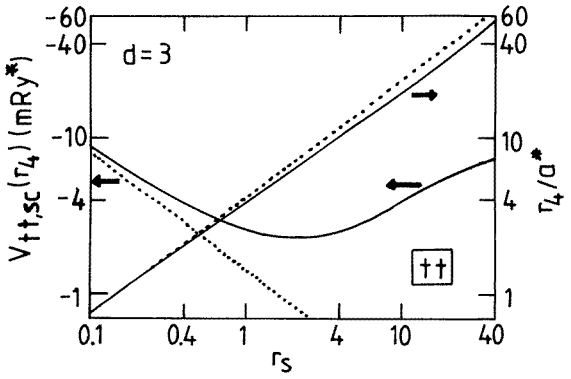

Figure 5. $V_{tt,sc}(r_4)$ and r_4 versus r_s for 3D as solid lines. The dotted lines represent $V_{RPA}(r_4)$ and r_4 within the RPA according to equation (11).

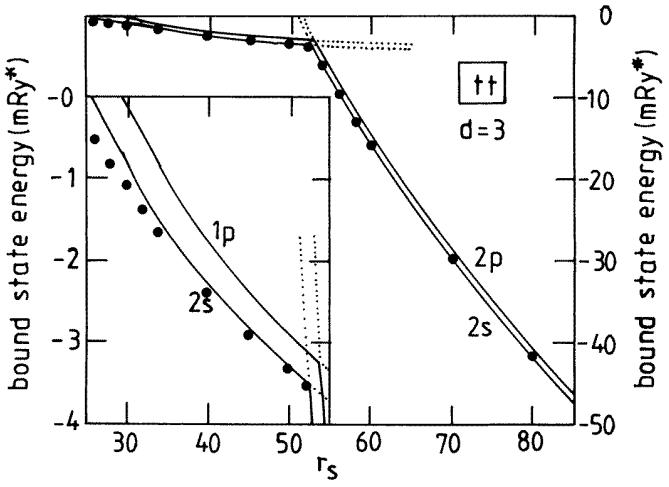

Figure 6. Binding energy for the 2s- and the 2p-state versus r_s for the tt-interaction in 3D from the variational calculation as solid lines. For $r_s < 52$ ($r_s > 52$) an oscillator wave function gives a larger (smaller) binding energy than a hydrogenic wave function. Our results from the matrix diagonalization for the 2s state are shown as solid points.

This suggested that the minimum of the potential at r_4 might induce excited bound states localized at r_4. Such states are better characterized by a variational harmonic oscillator wave function [5]

$$\phi_{4v}(r) = Ar^{k_1/2}\exp(-r^2/2\alpha^2) \tag{12a}$$

with $l = 1, 2, \ldots$ The variational parameters are k_1 and α. We denote these states $1p, 1d, \ldots$ because $\phi_{4v}(r)$ has one node for $k_1 > 0$. In order to describe states with two nodes and $l = 0$, which corresponds to the 2s state, we use [5]

$$\phi_{5v}(r) = B(r^{k_2/2} - Cr^{k_3/2})\exp(-r^2/2\beta^2). \tag{12b}$$

The variational parameters are k_2, k_3 and β.

The binding energies for the 2s and the 1p state versus r_s are shown in figure 6. For $r_s < 52$ the binding energies for the 2s state agree very well with the results of the matrix diagonalization method. However, for $r_s > 52$ the binding energies obtained with oscillator-like wave functions were too small compared with the exact result. With hydrogenic-like

wave function (2s and 2p) we found for $r_s > 52$ perfect agreement with the results of the matrix diagonalization method for the 2s state. We conclude that for $r_s < 52$ the Coulomb singularity at $r = 0$ is not strong enough to produce excited states and excited states are due to the minimum $V_{tt,sc}(r_4)$. However, for $r_s > 52$ the excited states are hydrogenic-like states.

4. Results for two dimensions

4.1. The screened potential

In 2D the screened Coulomb interaction in the real space is given by

$$V_{sc}(r) = \frac{1}{2\pi}\int_0^\infty \mathrm{d}q\, q\, J_0(qr) V_{sc}(q). \tag{13}$$

$J_0(x)$ is the zero-order Bessel function of the first kind.

Within the RPA in equation (13) and putting $x = rq_2$ one obtains for the screened potential

$$V_{RPA}(x) = -\frac{2\mathrm{Ry}^*}{r_s^{2/3}}\left\{\frac{1}{x} - 2\int_0^\infty \mathrm{d}y\, J_0(yx)/(1+y^3)\right\}. \tag{14}$$

The integral in equation (14) can be calculated analytically; it is expressed in terms of Bessel and Struve functions. The energy scale of $V_{RPA}(x)$ depends on $\mathrm{Ry}^*/r_s^{2/3}$, while the characteristic length r_0 is given by $x_0 = r_0 q_2 \approx 1$: $r_0 \approx 1/q_2 \propto r_s^{2/3}$. As for 3D we find that $V_{RPA}(r)$ is characterized by (i) a bare Coulomb attraction at small distances, (ii) a reduction due to screening at intermediate distances and (iii) oscillations at large distances.

$V_{RPA}(r)$ shows a Coulomb singularity for $r \to 0$, $V_{RPA}(r_1) = 0$ for

$$r_1/a^* = 0.586 r_s^{2/3} \tag{15a}$$

it has a maximum $V_{RPA}(r_2)/\mathrm{Ry}^* = 0.384/r_s^{2/3}$ for $r_2/a^* = 0.956 r_s^{2/3}$, it vanishes again $V_{RPA}(r_3) = 0$ for $r_3/a^* = 3.302 r_s^{2/3}$ and it shows a minimum

$$V_{RPA}(r_4)/\mathrm{Ry}^* = -0.001\,670/r_s^{2/3} \tag{15b}$$

for

$$r_4/a^* = 3.816 r_s^{2/3}. \tag{15c}$$

$V_{sc}(r)$ versus r is shown in figure 7 for $r_s = 2$. We conclude that in 2D many-body effects are already very important for $r_s = 2$. r_1 and r_2 are visible in figure 7.

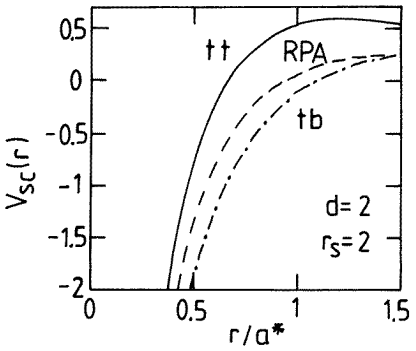

Figure 7. Screened potential $V_{sc}(r)$ versus distance r for $r_s = 2$ in 2D. The solid and dashed-dotted line represents the test-charge–test-charge (tt) and the test-charge–boson (tb) interaction, respectively. The dashed line represents the RPA.

4.2. Bound states within the RPA

The binding energies of the 1s state and the 2s and 2p states for some large r_s values are given in table 2 for boson screening and electron screening. For $r_s \gg 1$ the binding energies are nearly identical. As in the 3D case, this means that the quantum liquid statistics is almost irrelevant at very low densities.

Table 2. Binding energies in 2D for the 1s, 2s and 2p state found by the variational method within the RPA for screening by charged bosons and by charged fermions [5]. In the last row we give the values r_{sc} where the binding energy vanishes.

	Boson binding energy (Ry*)			Fermion binding energy (Ry*)		
r_s	1s	2s	2p	1s	2s	2p
0.8	−0.136	—	—	−0.691	—	—
1	−0.418	—	—	−0.802	—	—
2	−1.390	—	—	−1.432	—	—
5	−2.447	—	—	−2.411	—	—
10	−2.990	—	—	−2.966	—	—
30	−3.504	−0.030	−0.016	−3.496	−0.024	−0.009
40	−3.589	−0.085	−0.076	−3.584	−0.080	−0.071
100	−3.776	−0.232	−0.229	−3.774	−0.230	−0.228
1000	−3.952	−0.396	−0.396	−3.952	−0.396	−0.396
r_{sc}	0.703	25.7	27.9	0	26.6	28.8

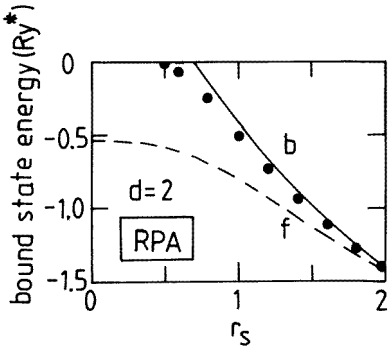

Figure 8. Binding energy for the 1s state versus r_s within the RPA for charged boson (solid line) and charged fermion (dashed line) screening in 2D from the variational calculation. Our results from the matrix diagonalization are shown as solid points.

At high density $r_s < 2$, the BC screening is more efficient than the electron screening and the binding energy vanishes at the critical density parameter $r_{sc} = 0.70$; see figure 8. In fact, for electron screening the binding energy remains finite at any density and tends to -0.56Ry^* for small r_s [8]. The 2D Mott's critical density N_{2c}, defined by $N_{2c}^{1/2}a^* = 1/\pi^{1/2}r_{sc}$, results in $N_{2c}^{1/2}a^* = 0.80$ for the 1s state. For the excited states the values of r_{sc} are given in table 2.

4.3. Bound states including many-body effects: tb

In figure 9 we show for the 1s state the effect of LFC on the binding energy. In 2D the binding energy of the unscreened hydrogenic impurity is -4Ry^* with $\nu = a^*/4$ for the ground state.

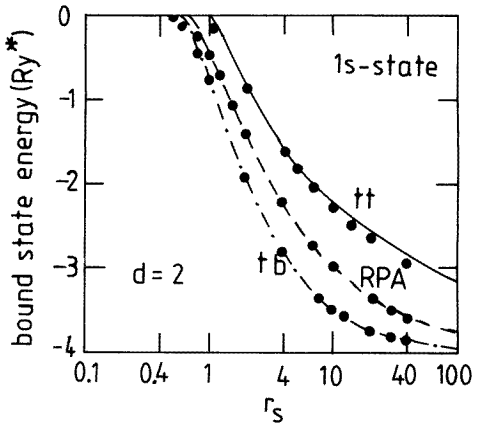

Figure 9. Binding energy for the 1s state versus r_s within the RPA (dashed line), the tb-interaction (dashed–dotted line) and the tt-interaction (solid line) in 2D from the variational calculation. Our results from the matrix diagonalization are shown as solid points.

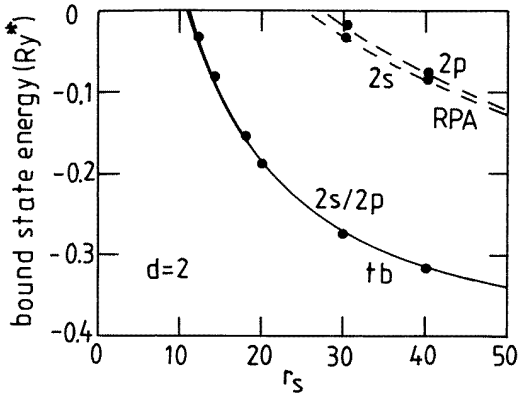

Figure 10. Binding energy for the 2s and the 2p state versus r_s for the tb-interaction and the RPA in 2D from the variational calculation. Our results from the matrix diagonalization are shown as solid points.

This value is obtained for $r_s \to \infty$ or $q_2 \to 0$. The LFC increases the binding energy for the tb-interaction compared with the RPA. Correspondingly, the parameter r_{sc} is smaller for the tb-interaction than within the RPA.

The results for excited states are shown in figure 10. r_{sc} is much higher for the excited states than for the ground state. For $r_s \to \infty$ one gets the 2D bare Coulomb potential and the energy of the first excited bound states is $-4\mathrm{Ry}^*/9$ with $\kappa = \mu = 3a^*/4$.

The variational parameters ν, κ and μ increase with decreasing r_s. Within the RPA and for the 1s state, ν increases from $a^*/4$ for $r_s \to \infty$ to $0.43a^*$ for $r_s = r_{sc} = 0.70$.

4.4. Bound states with the local-field correction: tt

The results of the 1s state calculations for the tt-interaction are shown in figure 9. The binding energies are smaller than within the RPA. The 1s state is described by the hydrogenic-like wave function.

The excited states calculations are somewhat more involved than for the tb-interaction. Using the variational wave function $\phi_{2v}(r)$ and $\phi_{3v}(r)$ for the hydrogenic 2s and the 2p states, we obtained binding energies a factor of ten smaller than found within the diagonalization method. The variational parameters κ and ν were found to be anomalously large. This suggested to us that the excited states are more extended than what would be expected for 2D 'hydrogen' states and that another variational form for the wave function should be used. As in 3D, we also found in 2D that the LFC strongly deepens the minimum of the screened potential $V_{tt,sc}$ at $r = r_4$ compared to the RPA result; see figure 11 and compare with $V_{RPA}(r_4)/\mathrm{Ry}^* = -0.001\,670/r_s^{2/3}$, which cannot be shown on the scale used in figure 11.

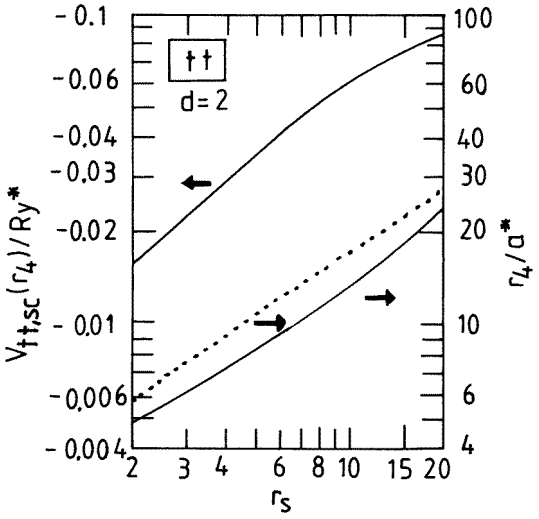

Figure 11. $V_{tt,sc}(r_4)$ and r_4 versus r_s for 2D as solid lines. The dotted line represents r_4 within the RPA according to equation (15*c*).

This means that $V_{tt,sc}(r)$ leads to very extended excited states where the particle is localized near r_4. Such states are better characterized by a variational harmonic oscillator wave function [5] $\phi_{4v}(r)$ with $l = 1, 2, \ldots$. In order to describe the 2s state, we use [5] $\phi_{5v}(r)$, see equation (12).

The excited-state binding energies obtained with the wave functions $\phi_{4v}(r)$ and $\phi_{5v}(r)$ versus r_s are shown in figure 12. The number of excited states 1p, 1d, 1e,... increases strongly with increasing r_s. This is because $V_{eff}(r)$ defined in section 2.3 becomes flatter around its minimum $r \approx r_4 \gg a^*$. Note that the 2s state has a larger binding energy than the 1p state. A very good agreement is found between the matrix diagonalization method and the variational method.

5. Discussion

5.1. General

This paper presents an extensive study of binding energies for the tt- and the tb-interaction as a function of the charged BC density. The general expression of the screened potentials is

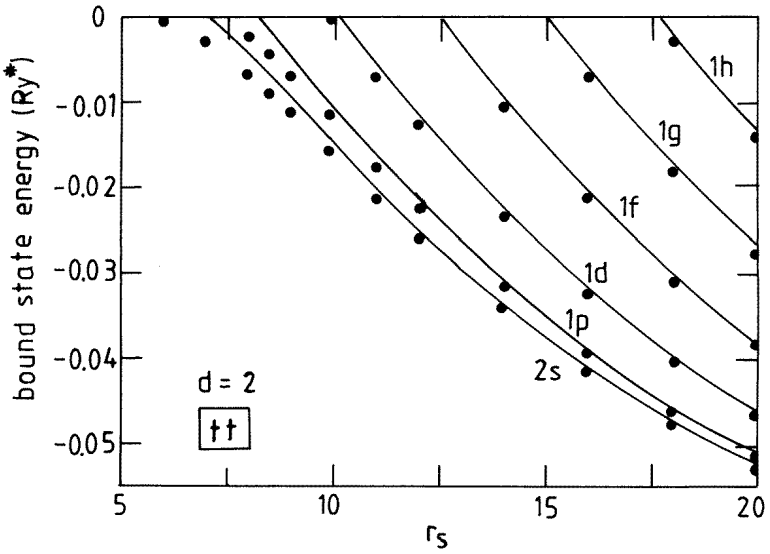

Figure 12. Binding energy for excited states versus r_s in 2D for the test-charge–test-charge interaction using oscillator-like wave functions. The solid dots are the results obtained by matrix diagonalization.

cumbersome and non-analytic and conveys different behaviours according to the distance from the centre. Therefore, the results given for $V_{RPA}(r)$ are useful (i) to clarify these behaviours, (ii) to characterize bound states in a non-trivial potential and (iii) to identify this potential as a Coulomb potential screened by a charged BC.

The comparison of results for the binding energies obtained by the exact diagonalization method with the variational method shows that the much simpler variational method gives very good results not only for the ground state but also for excited states. Only for small binding energies near r_{sc} does the variational method give binding energies substantially smaller than the exact matrix diagonalization method, see figure 2 and figure 8.

At low enough densities, no significant difference is found between boson screening and electron screening; see table 1 and table 2. For the Bose condensate in 3D the screening function is given by $\varepsilon_{RPA}(q) = 1 + q_3^4/q^4$. For the electron gas in 3D one finds $\varepsilon_{RPA}(q \ll 2k_F) = 1 + 4k_F/a^*q^2 = 1 + q_{TF3}^2/q^2$ and $\varepsilon_{RPA}(q \gg 2k_F) = 1 + q_3^4/q^4$. k_F is the Fermi wave number and q_{TF3} is the Thomas–Fermi screening wavenumber in 3D. For the Bose condensate in 2D the screening function is given by $\varepsilon_{RPA}(q) = 1 + q_2^3/q^3$. In 2D one finds for the electron gas $\varepsilon_{RPA}(q \ll 2k_F) = 1 + 2/a^*q = 1 + q_{TF2}/q$ and $\varepsilon_{RPA}(q \gg 2k_F) = 1 + q_2^3/q^3$. Because of the agreement of the binding energies we conclude that for large r_s the binding energies of the electron gas are determined by $\varepsilon_{RPA}(q \gg 2k_F)$ and the screening functions of an electron gas and a Bose condensate are identical for large wave numbers. This means that for an electron gas and for large r_s the binding energy of a screened impurity is determined by q_d, as for a Bose condensate, independent of q_{TFd}.

This is explained by the fact that bound states are short-distance phenomena, where the dielectric function for boson screening is identical to the dielectric function for electron screening. These arguments can also be applied to the tb-interaction and the tt-interaction because the difference between the LFC for electron and boson systems becomes small for large r_s [27].

5.2. Unexpected results

We found two unexpected results. Screening effects of a 2D-BC may be strong enough to make the binding energy of a hydrogenic state vanish; see figure 8 and figure 9. This is a qualitative new behaviour as compared to 2D electron screening, where the binding energy remains finite [8]. It was sometimes argued in the literature that a bound state exists in 2D whenever there is an attractive potential, independently of its strength. In fact, this is only true for a short-range potential. For a long-range potential we conclude from the present study that for $r_s < r_{sc}$ even a Coulomb attraction at small distances is not sufficient to guarantee a bound state in the presence of charged BC screening.

The results shown in figure 12 for the tt-interaction indicate that the nature of excited states in 2D changes if the LFC is taken into account. Within the variational calculation using the 2s and the 2p variational wave function of hydrogen type, the very large values obtained for the variational parameters indicated that some qualitative new phenomenon must occur for the tt-interaction. In fact, the variational calculation with Gaussian envelope wave functions was found to be in good agreement with the numerical results, pointing to the oscillator nature of the effective potential for the excited states.

For the tt-interaction in 3D we did not find excited bound states for $r_s < 22$. It might be quite interesting for statistical mechanics to know that in a large density range ($0 < r_s < 22$) only one bound state exists and excited states are absent. Our results for the excited states of the tt-interaction in 3D for $r_s > 22$, shown in figure 6, and the transition from oscillator-like wave functions to hydrogenic-like wave functions with increasing r_s illustrates the power of the variational approach.

We also mention that according to our knowledge excited states for the tt-interaction in 3D have not yet been studied for electron screening. We expect that a similar behaviour for excited states as found for boson screening occurs in systems with electron screening.

5.3. Critical density parameter r_{sc}

In table 3 we summarize the values for r_{sc} where the binding energy for the ground state and the excited states vanishes. The values of r_{sc} for 2D are smaller than for 3D, which indicates that screening effects are less efficient in 2D than in 3D. We also notice that the r_{sc}-values obtained with the matrix diagonalization method are smaller than the r_{sc}-values obtained with the variational method. The results given in table 3 are calculated with hydrogenic variational wave functions.

Table 3. Critical Wigner–Seitz parameter r_{sc} for the 1s, 2s and 2p state found by the variational method for 2D and 3D, within RPA, the tb- and the tt-interaction. The values in brackets represent our results for r_{sc} for the 1s state obtained using the matrix diagonalization method.

	r_{sc} for $d = 3$			r_{sc} for $d = 2$		
	1s	2s	2p	1s	2s	2p
test–test (tt)	3.13 [2.7]	50.6	52.3	1.01 [0.6]	7.1	11.3
RPA	2.60 [2.23]	16.9	18.8	0.70 [0.35]	25.7	27.9
test–boson (tb)	2.33 [2.1]	12.3	13.1	0.62 [0.3]	10.8	10.9

The r_{sc}-values given in table 4 for the tt-interaction in 3D and 2D represent, for the excited states, the values obtained with the oscillator variational wave functions; see figure 6 for 3D and figure 12 for 2D.

Table 4. Critical Wigner–Seitz parameter r_{sc} for the 1s, 2s and 1p state found by the variational method for 3D and 2D for the test-charge–test-charge interaction. The 2s and 1p state corresponds to oscillator variational wave functions. The values in brackets represent our results obtained using the matrix diagonalization method, see figure 6 for 3D and figure 12 for 2D.

State	1s	2s	1p
r_{sc} for tt for $d = 3$	3.13 [2.7]	25.5 [22]	29
r_{sc} for tt for $d = 2$	1.01 [0.6]	7.1 [6.0]	8.2 [7.5]

With the r_{sc}-value one can calculate the Mott density N_{dc}. The different values of r_{sc} for the RPA, the tb- and the tt-interactions are due to exchange–correlation effects as given by the LFC. To our knowledge, the existence of such critical densities for binding with charged boson screening has never been studied in the literature. We found that the charged BC screening is stronger than the electron screening under the same conditions of dimensionality and gas density.

5.4. Application

The calculation of the screened potential, see figure 1 and figure 7, demonstrates that for $r_s > 1$ the LFC must be taken into account in order to give a realistic description of the interaction potential. Many-body effects are somewhat stronger in 2D than in 3D.

Our calculation is of interest to understand the difference between electron and boson screening, studied as the reduction of the binding energies of hydrogenic impurities. If we take the charged BC as a simple model to describe a superconductor we conclude from our calculations that the binding energies for large r_s are not modified by the presence of a BC. However, the Mott density is modified, especially if we consider a 2D system.

The presence of a BC might be the origin in a hypothetical experiment on a 2D electron system where the vanishing of the binding energy is observed for $r_s < r_{sc} \approx 0.4$.

We also have considered the case of two equally charged test-particles screened by a Bose condensate. The results of these calculations are reported elsewhere [28].

6. Conclusion

We discussed screening effects on hydrogenic bound states due to a charged Bose condensate in three and two dimensions. Screening effects of the Bose condensate reduce the binding energy of the hydrogenic bound states. The random-phase approximation, the test-charge–boson and test-charge–test-charge interactions were discussed in detail.

In the very dilute limit (for very low density), the differences in binding energies with electron or boson screening are small. However, when the binding energy becomes small (for higher density), boson screening is found to be more efficient than electron screening. In addition, with charged Bose condensate screening, no bound state exists beyond a critical density in both 3D and 2D.

References

[1] Mott N F 1949 *Proc. Phys. Soc.* **162** 416
[2] Krieger J B and Nightingale M 1971 *Phys. Rev.* B **4** 1266
[3] Greene R L, Aldrich C and Bajaj K K 1977 *Phys. Rev.* B **15** 2217
Aldrich C 1977 *Phys. Rev.* B **16** 2723
Borges A N O, Hipólito O and Campos V B 1995 *Phys. Rev.* B **52** 1724

[4] Neethiulagarajan A and Balasubramaniam S 1983 *Phys. Rev.* **28** 3601
[5] Gold A and Ghazali A 1996 *J. Phys.: Condens. Matter* **8** 7393
Gold A and Ghazali A 1997 *J. Phys.: Condens. Matter* **9** 3749
Gold A and Ghazali A 1997 *J. Phys.: Condens. Matter* **9** 6885
[6] Bulutay C, Al-Hayek I and Tomak M 1997 *Phys. Rev.* B **56** 15 115
[7] Bastard G 1980 *Phys. Rev.* B **24** 4714
[8] Brum J A, Bastard G and Guillemot C 1984 *Phys. Rev.* B **30** 905
[9] Hipólito O and Campos V P 1979 *Phys. Rev.* B **19** 3083
Gold A 1989 *Z. Phys.* B **74** 53
Ackleh E S, Mahan G D and Wu J-W 1994 *Mod. Phys. Lett.* **8** 1041
[10] Gold A 1992 *Physica* C **190** 483
Alexandrov A S and Mott N F 1993 *Supercond. Sci. Technol.* **6** 215
[11] Jetzer P 1992 *Phys. Rep.* **220** 163
[12] Mewes M O, Andrews M R, van Druten N J, Kurn D M, Durfee D S, Townsend C G and Ketterle W 1996 *Phys. Rev. Lett.* **77** 988
[13] Lee J C 1975 *Phys. Rev.* B **12** 2644
Hore S R and Frankel N E 1975 *Phys. Rev.* B **12** 2619
[14] Hansen J P and Mazighi 1978 *Phys. Rev.* A **18** 1282
[15] Caparica A A and Hipólito O 1982 *Phys. Rev.* A **26** 2832
[16] Sugiyama G, Bowen C and Alder B J 1992 *Phys. Rev.* B **46** 13 042
[17] Conti S, Chiofalo M L and Tosi M P 1994 *J. Phys.: Condens. Matter* **6** 8795
[18] Moroni S, Conti S and Tosi M P 1996 *Phys. Rev.* B **53** 9688
[19] Gold A 1992 *Z. Phys.* B **89** 1
[20] Kim H K, Tao R and Wu F Y 1979 *Phys. Rev.* B **34** 7123
[21] Moudgil R K, Ahluwalia P K, Tankeshwar K and Pathak K N 1997 *Phys. Rev.* B **55** 544
[22] Mahan G D 1990 *Many-Particle Physics* (New York: Plenum)
[23] Kukkonen C A and Overhauser A W 1979 *Phys. Rev.* B **20** 550
[24] Singwi K S and Tosi M P 1981 *Solid State Physics* vol 36 (New York: Academic) p 177
[25] Gold A 1997 *Z. Phys.* B **103** 491
[26] Gold A to be published
[27] Gold A 1994 *Phys. Rev.* B **50** 4297
[28] Gold A and Ghazali A 1999 *J. Phys.: Condens. Matter* **11** 2379